### Title

Modest Decreases in Endogenous All-Trans-Retinoic Acid Produced by a Mouse Rdh10 Heterozygote Provoke Major Abnormalities in Adipogenesis and Lipid Metabolism




### Journal

Diabetes, 67(4)

### ISSN

0012-1797



### Authors

Yang, Di
Vuckovic, Marta G
Smullin, Carolyn P
et al.



### Publication Date

2018-04-01

### DOI

10.2337/db17-0946

Peer reviewed

# Modest Decreases in Endogenous All-*trans*-Retinoic Acid Produced by a Mouse *Rdh10* Heterozygote Provoke Major Abnormalities in Adipogenesis and Lipid Metabolism

Di Yang,[1,2] Marta G. Vuckovic,[2] Carolyn P. Smullin,[2] Myeongcheol Kim,[2] Christabel Pui-See Lo,[2] Emily Devericks,[2] Hong Sik Yoo,[2] Milena Tintcheva,[2] Yinghua Deng,[2] and Joseph L. Napoli[1,2]

*Diabetes* 2018;67:662–673 | https://doi.org/10.2337/db17-0946

**Pharmacological dosing of all-*trans*-retinoic acid (atRA) controls adiposity in rodents by inhibiting adipogenesis and inducing fatty acid oxidation. Retinol dehydrogenases (Rdh) catalyze the first reaction that activates retinol into atRA. This study examined postnatal contributions of Rdh10 to atRA biosynthesis and physiological functions of endogenous atRA. Embryonic fibroblasts from *Rdh10* heterozygote hypomorphs or with a total *Rdh10* knockout exhibit decreased atRA biosynthesis and escalated adipogenesis. atRA or a retinoic acid receptor (RAR) panagonist reversed the phenotype. Eliminating one *Rdh10* copy in vivo (*Rdh10*$^{+/-}$) yielded a modest decrease (≤25%) in the atRA concentration of liver and adipose but increased adiposity in male and female mice fed a high-fat diet (HFD); increased liver steatosis, glucose intolerance, and insulin resistance in males fed an HFD; and activated bone marrow adipocyte formation in females, regardless of dietary fat. Chronic dosing with low-dose atRA corrected the metabolic defects. These data resolve physiological actions of endogenous atRA, reveal sex-specific effects of atRA in vivo, and establish the importance of Rdh10 to metabolic control by atRA. The consequences of a modest decrease in tissue atRA suggest that impaired retinol activation may contribute to diabesity, and low-dose atRA therapy may ameliorate adiposity and its sequelae of glucose intolerance and insulin resistance.**

OBESITY STUDIES

All-*trans*-retinoic acid (atRA) controls proliferation, differentiation, and cell function by regulating multiple genes through the following nuclear receptors: retinoic acid receptor (RAR)α, -β, and -γ and PPARδ (1). Two reactions generate atRA from vitamin A (retinol). Retinol dehydrogenases (Rdh) of the short-chain dehydrogenase/reductase gene family (Rdh1, Rdh10, and Dhrs9) convert retinol into retinal, whereas retinal dehydrogenases (Raldh) of the aldehyde dehydrogenase gene family (Raldh1, -2, and -3) convert retinal into atRA (2,3). Retinal reductases (e.g., Dhrs3) also contribute to maintaining steady-state retinal concentrations, as does carotenoid cleavage (4). atRA concentrations are maintained by the steady-state concentration of retinal set by Rdh and reductases and activities of Raldh and atRA catabolic enzymes (Cyp26A1, -B1, and -C1) (5,6). The distinct but overlapping spatial and temporal expression patterns of *Rdh* suggest that specific isoforms satisfy discrete functions (7). Differences in the phenotypes of ablated retinoid metabolon proteins provide further support for this hypothesis (8,9).

*Rdh10* was cloned from the retinal pigment epithelium and retinal Muller cells as an all-*trans*- and 11-*cis*-Rdh in the visual cycle (10,11). *Rdh10*, however, has widespread expression during embryogenesis, localizing with many sites of atRA signaling (12). Most homozygous *Rdh10*-null mouse pups die by embryo day 13 (E13) from severe forelimb, internal organ, and forebrain abnormalities (13). Long-term retinal dosing to dams allows the birth of *Rdh10*-null mice in Mendelian frequency but does not rescue all aspects of atRA deficiency in neonates. An Rdh10 hypomorph, produced by a missense mutation (A196V), produces pups that die mostly by E17.5 with edema, a midline facial cleft, forebrain defects, impaired cerebrovasculature, and absence

[1]Graduate Program in Metabolic Biology, University of California, Berkeley, Berkeley, CA
[2]Department of Nutritional Sciences and Toxicology, University of California, Berkeley, Berkeley, CA
Corresponding author: Joseph L. Napoli, jna@berkeley.edu.

Received 9 August 2017 and accepted 2 January 2018.

This article contains Supplementary Data online at http://diabetes.diabetesjournals.org/lookup/suppl/doi:10.2337/db17-0946/-/DC1.

C.P.S. and M.K. contributed equally to this work.

of olfactory bulbs (14,15). Thus, atRA production during mid-to-late gestation requires Rdh10, but additional Rdh also are important during embryogenesis.

Postnatal contributions of Rdh10 to atRA biosynthesis have not been studied extensively. A Sertoli and/or germ cell–specific *Rdh10* knockout in juvenile mice prevents spermatogenesis equivalent to that during vitamin A deficiency, but upon reaching adulthood, these mice exhibit normal spermatogenesis, indicating age-specific Rdh10 functions (16). Overexpression of *Rdh10* in primary human neonate keratinocytes produced an aberrant phenotype, consistent with the inhibition of differentiation and upregulation of atRA-induced genes (17). The same phenomena were not duplicated by overexpression of the human ortholog (*RDH16*) of mouse *Rdh1,* suggesting that Rdh10 serves as the major Rdh in neonate keratinocytes. In contrast, sequential knockdown of endogenous Rdh in primary rat hippocampus astrocytes showed that Rdh10, Dhrs9, and Rdh2 (rat ortholog of mRdh1) contribute to atRA biosynthesis (18).

The *mRdh1* knockout illustrates the contribution of endogenous atRA to energy balance (19). When fed a low-fat diet (LFD), *mRdh1*-null mice have a 59% (12.7 g) increase in fat at 36 weeks old relative to wild type (WT). *Rdh1*-null mice, however, do not have other symptoms of atRA deficiency. Pharmacological atRA dosing to mice fed high-fat diets (HFDs) further suggests that retinoids regulate energy balance and adiposity postnatally (20,21).

This study was undertaken to determine postnatal contributions of Rdh10 to atRA biosynthesis and function. We used heterozygous knockouts ($Rdh10^{+/-}$) and embryonic fibroblasts from *Rdh10* hypomorphs to study the impact of Rdh10 on atRA generation and function. Heterozygotes were used to circumvent homozygote embryonic lethality. Knocking out one *Rdh10* copy yielded only a modest decrease in tissue atRA but produced an array of metabolic and tissue abnormalities, some of which were sex specific. These results reveal Rdh10 contributions to atRA metabolic functions, resolve physiological actions of endogenous atRA in vivo and its sex-specific effects, and predict health consequences of a modest decrease in tissue atRA.

## RESEARCH DESIGN AND METHODS

### Mice

*Rdh10*-targeted C57BL/6N embryonic stem cells were injected into BALB/C blastocysts by the University of California (UC) Davis Mouse Biology Program with loxP sites that flank *Rdh10* exon 2 (Supplementary Fig. 1). *Rdh10* floxed mutants were back-crossed into C57BL/6J mice >12 generations and bred with mice expressing CMV-Cre [B6.C-Tg(CMV-cre)1Cgn/J; The Jackson Laboratory] to generate $Rdh10^{+/-}$ mice. Controls were littermates ($Rdh10^{+/+}$ and $CMV\text{-}Cre^{+}$).

Mice were fed an AIN93G diet with 4 IU/g vitamin A (180614; Dyets, Inc) and 9% fat (LFD) or 50% fat as lard (HFD). Unless noted otherwise, mice were 4 months old and fed either diet from weaning. Body and food weights were measured weekly. Body composition was determined with an EchoMRI 100V whole-body magnetic resonance analyzer. Energy expenditure and activity were assessed with a laboratory animal monitoring system. $VO_2$ and $VCO_2$ were normalized to the lean body mass of each mouse. Femur marrow was harvested by centrifugation (22). Animal experiments were performed in accordance with the National Institutes of Health's Guide for the Care and Use of Laboratory Animals. Protocols were approved by the UC Animal Care and Use Committee.

### atRA Dosing

Five milligrams of 90-day slow-release atRA pellets or placebo (Innovative Research of America) were implanted under the skin on the lateral side of the neck in 6-week-old mice.

### Glucose Tolerance Test/Insulin Tolerance Test

Glucose tolerance tests (GTTs) and insulin tolerance tests (ITTs) were performed on 4-month-old mice fed an HFD. Mice were fasted 16 h before GTT and 4 h before ITT and placed in individual cages without food, but with free access to water. Either glucose (1.5 g/kg body weight) or insulin (0.5 IU/kg body weight) was injected. Blood glucose from tail tips was measured with a glucometer.

### Serum Measurements

Serum was sent to the UC Davis Mouse Metabolic Phenotyping Center for quantification of insulin, leptin, adiponectin, and β-hydroxybutyrate. Serum nonesterified fatty acid (NEFA) was quantified with an EnzyChrom Free Fatty Acid Assay Kit (EFFA-100).

### TAG Assay

Triacylglycerol (TAG) was measured in homogenized livers using a Triglyceride Colorimetric Assay Kit (10010303; Cayman Chemical). Values were normalized to liver wet weight.

### Quantitative PCR

mRNA expression was normalized to the geometric means of *Gusb* and *Tbp*. Primer and quantitative PCR details are included in the Supplementary Data.

### Histology

Formalin-fixed, paraffin-embedded tissues were cut into 8-μm sections. Deparaffinized sections were stained with hematoxylin-eosin (H-E). Fibrosis was visualized with Lillie's modified Masson's Trichrome Stain for Connective Tissue. Tissue sections were imaged using a Zeiss Axio Imager M1 microscope equipped with QImaging 5MPix MicroPublisher.

### F4/F80 Immunohistochemistry

Liver was embedded in Tissue-Tek optimal cutting temperature compound (OCT), snap frozen in liquid nitrogen, and sectioned into 12-μm slices. Slides were fixed by submersion in ice-cold acetone. Endogenous peroxidase was blocked with 0.3% $H_2O_2$. Slides were incubated with F4/80 antibody (Immunocruz ABC Staining System) and counterstained in H-E.

### Bone Histology

Femurs were fixed for 24 h at 4°C in Bouin solution (50:1) and decalcified in 10% EDTA at 4°C. Femurs were bisected

at the diaphysis center into proximal and distal halves. Distal femurs were dehydrated, embedded in paraffin, and sectioned longitudinally starting 10 μm from the frontal (coronal) plane. Sections 50–150 were collected onto Premiere Charged Microscope slides in a water bath at 40–42°C and H-E stained.

### Liver Oil Red O Staining

Liver was embedded in OCT in cryostat molds, snap frozen in liquid nitrogen, sectioned at 12 μm, fixed with 10% neutral-buffered formalin, submerged in Oil Red O, and counterstained in Harris Modified Hematoxylin Solution. Sections were treated with aqueous mounting medium (Shurmount). Slides were imaged within 24 h to avoid interference from Oil Red O precipitation.

### Mouse Embryonic Fibroblasts

Mouse embryonic fibroblasts (MEFs) were isolated from E13.5–14 embryos (23) and cultured in ultraviolet-irradiated growth medium of DMEM (Gibco BRL), 10% bovine calf serum (30-2030; American Type Culture Collection), and 100 units/mL penicillin/streptomycin (Gibco BRL) in six-well plates at 37°C. Differentiation was induced 2 days after confluence (differentiation day 0 [dd0]), with growth medium containing 0.5 mmol/L methylisobutylxanthine (IBMX), 1 μmol/L dexamethasone, 0.85 μmol/L insulin, and 100 nmol/L rosiglitazone. After 3 days (dd3), the medium was changed to growth medium with 0.85 μmol/L insulin and 100 nmol/L rosiglitazone, renewed every other day. Each experiment was performed with MEFs from two to three dams and repeated two to three times with MEFs from different dams. MEFs from littermates were compared.

Effects of nuclear receptor ligands were tested with vehicle (DMSO), 500 nmol/L atRA (refreshed daily), 100 nmol/L TTNPB (RAR pan-agonist; T3757; Sigma-Aldrich), or 100 nmol/L GW0742 (PPARδ agonist; G3295; Sigma-Aldrich) (refreshed every 2 days).

atRA biosynthesis was quantified in MEFs treated for 2 h with 250 nmol/L retinol, a physiological concentration (24). Cells were collected with 1× reporter lysis buffer (E397A; Promega) and flash frozen. atRA was quantified by liquid chromatography with tandem mass spectrometry (25).

Oil Red O staining was performed on dd7. MEFs were fixed with 10% formalin/PBS and stained with 60% Oil Red O/isopropanol. Excess stain was removed by washing with water. Stained oil droplets were dissolved in isopropanol. Absorbance was read at 510 nm.

### MEF *Rdh10* Ablation

A guide RNA targeting exon 3 in a lentiCRISPR v2 plasmid (plasmid 52961; Addgene) was introduced into SV40-immortalized MEFs (26). Cells that survived puromycin selection were plated individually. DNA was sequenced for Cas9-induced breaks repaired by nonhomologous end joining. Both alleles of *Rdh10* were affected, resulting in deletion of exons 3 (active site) to 6, i.e., amino acid residues beyond 184. Colonies with random mutations were used as controls. The guide RNA sequence was as follows: forward 5′-CACCGACGATGCTAGAGATTAATCA-3′; reverse 5′-AAACTGATTAATCTCTAGCATCGTC-3′. The probe to verify CRISPR knockout was Mm.PT58/9541215. Four control and four knockdown clones were isolated (Supplementary Fig. 2). One clone of each was chosen for detailed study (WT6 and KO27).

### Statistics

Data are expressed as means ± SD, unless noted otherwise. Significance was determined by two-tailed, unpaired Student *t* tests or two-way ANOVA.

## RESULTS

### Rdh10 Generates atRA in Preadipocytes

*Rdh10* expression is >22-fold more intense than *Dhrs9* in primary undifferentiated MEFs (dd0) (Fig. 1*A*). *Rdh10* mRNA decreases by 50% after MEF differentiation, but *Dhrs9* mRNA does not change. *Rdh1* and *RdhE2* mRNA were not detected. The net atRA concentration in WT MEFs after incubation with retinol also decreases ~50% from dd0 during adipogenesis (Fig. 1*B*), suggesting that Rdh10 generates atRA to inhibit adipogenesis.

To test whether downregulation of *Rdh10* allows adipogenesis, we used a mouse model harboring a mutated Rdh10 ($Rdh10^{m366Asp}$), which encodes a hypomorph with lower activity than WT because of a single nucleotide mutation in the substrate binding pocket (V196A) (14). This model has the benefit of reducing catalytic activity without altering *Rdh10* expression, which avoids off-target effects that might result from gene ablation. Homozygous hypomorphs die before E13.5–14. Therefore, we isolated MEFs from heterozygous hypomorphs (HYPO). HYPO MEFs had a 40% reduction in the steady-state atRA concentration relative to WT after incubation with retinol (Fig. 1*C*). Only *Dhrs9* mRNA among retinoid metabolon genes compensated for the *Rdh10* ablation, with a twofold increase ($P < 0.03$) (Supplementary Fig. 3). Basal expression of *Pparg* in HYPO MEFs did not differ from WT on dd0 (Fig. 1*D*). After differentiation (dd7), HYPO MEFs had ~40% more adipocytes than WT (Fig. 1*E* and *F*); expression of adipogenic markers (*Pparg* and *aP2*) was ~2.5- to 3.8-fold higher in HYPO versus WT MEFs (Fig. 1*G*). Total knockout of *Rdh10* with CRISPR CAS9 in immortalized MEFs (CKO) revealed an ~18-fold increase in Oil Red O–positive cells compared with immortalized WT MEFs (Fig. 1*H–J*), with *Pparg* and *Fabp4* expression ~3-fold higher (Fig. 1*K*). These data are consistent with *Rdh10* generating atRA in mesenchymal stem cells to suppress adipogenesis.

Both HYPO and WT MEFs responded to increasing retinol concentrations, but HYPO MEFs differentiated to a greater extent than WT (Fig. 2*A*). The $IC_{50}$ values of retinol were 290 and 333 nmol/L for WT and HYPO, respectively, for Oil Red O quantification (Fig. 2*B*). The marked difference in total lipids, but the small difference between the $IC_{50}$ values, may result from Oil Red O reflecting total lipid accumulation, caused by both adipogenesis and de novo lipogenesis. The absolute values of Oil Red O concentrations

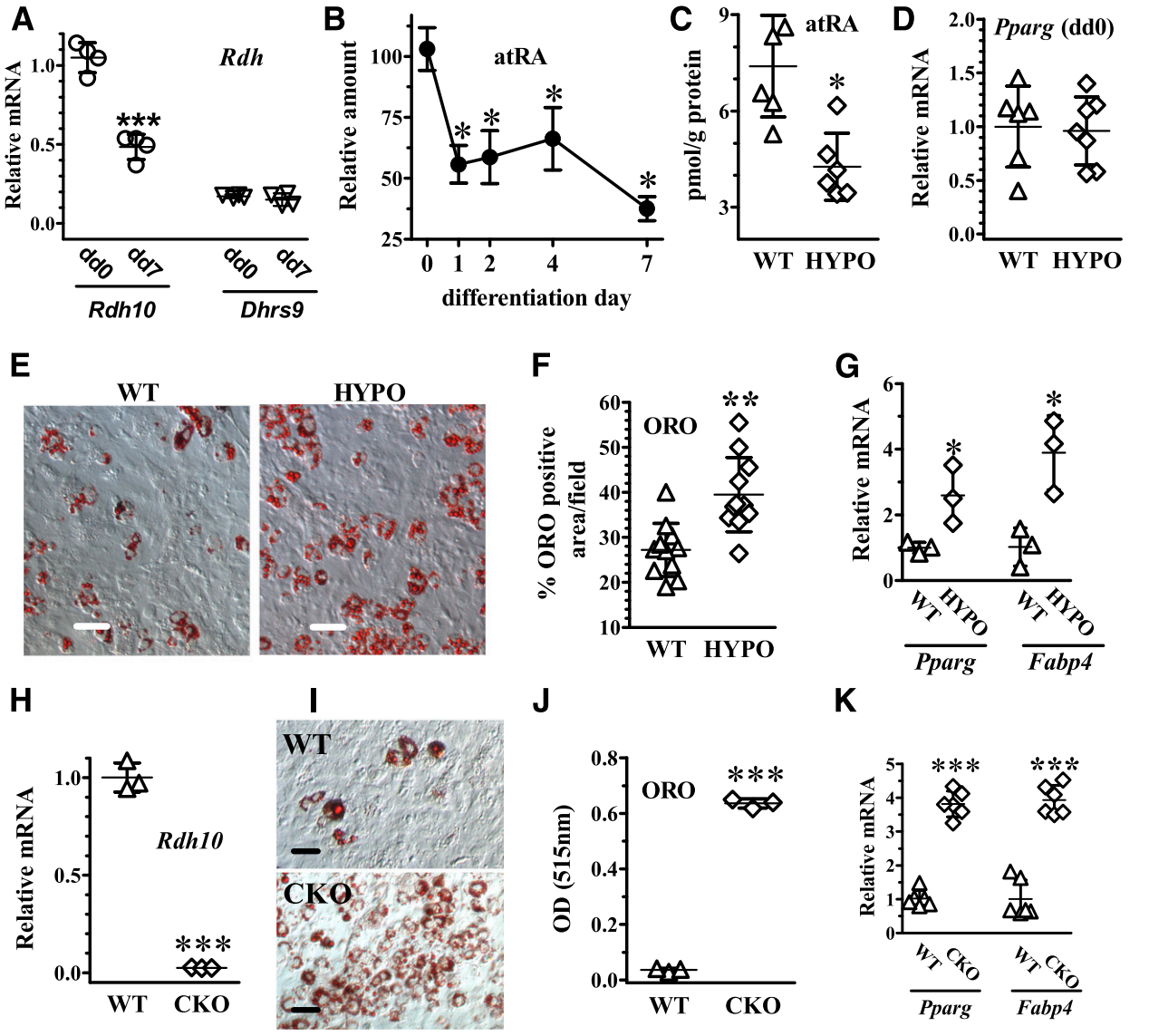


**Figure 1**—Rdh10 generates atRA in preadipocytes. *A*: Relative expression of *Rdh* in undifferentiated WT MEFs (dd0) or differentiated MEFs (dd7). MEFs from four to five embryos were assayed individually. ***$P < 0.001$. *B*: atRA concentrations during adipogenesis. WT MEFs were treated with 250 nmol/L retinol for 2 h on each dd. Data are combined from two experiments with MEFs from 6 to 11 embryos per time point ± SE. *$P < 0.05$, compared with dd0. *C*: atRA concentrations in WT vs. *Rdh10* HYPO mutant MEFs on dd0. Cells were treated for 2 h with 250 nmol/L retinol; MEFs from six embryos per group. Representative data from three experiments. *$P < 0.05$. *D*: *Pparg* mRNA in WT and *Rdh10* HYPO mutant MEFs (dd0). Data are combined from two experiments. *E*: Representative images of Oil Red O (ORO) staining of differentiated WT and *Rdh10* HYPO mutant MEFs (dd7). Representative data from three experiments. Scale bars, 50 μm. *F*: Quantification of data in *E*. Oil Red O–positive cell numbers were counted by two individuals independently. $n = 11$ embryos per genotype. **$P < 0.01$. Representative data from three experiments. *G*: Expression of adipogenic markers on dd7. MEFs from three embryos. *$P < 0.05$. *H*: *Rdh10* mRNA in WT and CKO on dd0. MEFs from three wells each. ***$P < 0.001$. *I*: Oil Red O images of differentiated WT and CKO MEFs on dd7. Scale bars, 50 μm. *J*: Quantification of data in *I*. MEFs from three wells per group per experiment. ***$P < 0.001$. Representative data from two experiments. OD, optical density. *K*: Expression of adipogenic markers on dd7 in WT and CKO MEF. MEFs from six wells for each genotype were assayed individually. Representative data from two experiments. ***$P < 0.001$.

would differ because of differences in adipogenesis, whereas the $IC_{50}$ values would reflect the distinct process of lipid accumulation in differentiated cells. The $IC_{50}$ values of adipocyte-expressing genes *Pparg* (454 and 915 nmol/L, respectively, for WT and HYPO) and *Ap2* (65 and 703) indicate enhanced adipogenesis associated with impaired HYPO atRA biosynthesis (Fig. 2*C* and *D*). Higher retinol concentrations produced differences in expression of atRA-inducible genes *Rarb*, *Cyp26a1*, and *Cyp26b1*, consistent with impaired HYPO atRA biosynthesis from retinol.

### *Rdh10*$^{+/-}$ Mice Have More Severe Diet-Induced Obesity and Insulin Resistance

To determine Rdh10 functions in vivo, we generated mice with a whole-body deletion. Heterozygotes (*Rdh10*$^{+/-}$) were

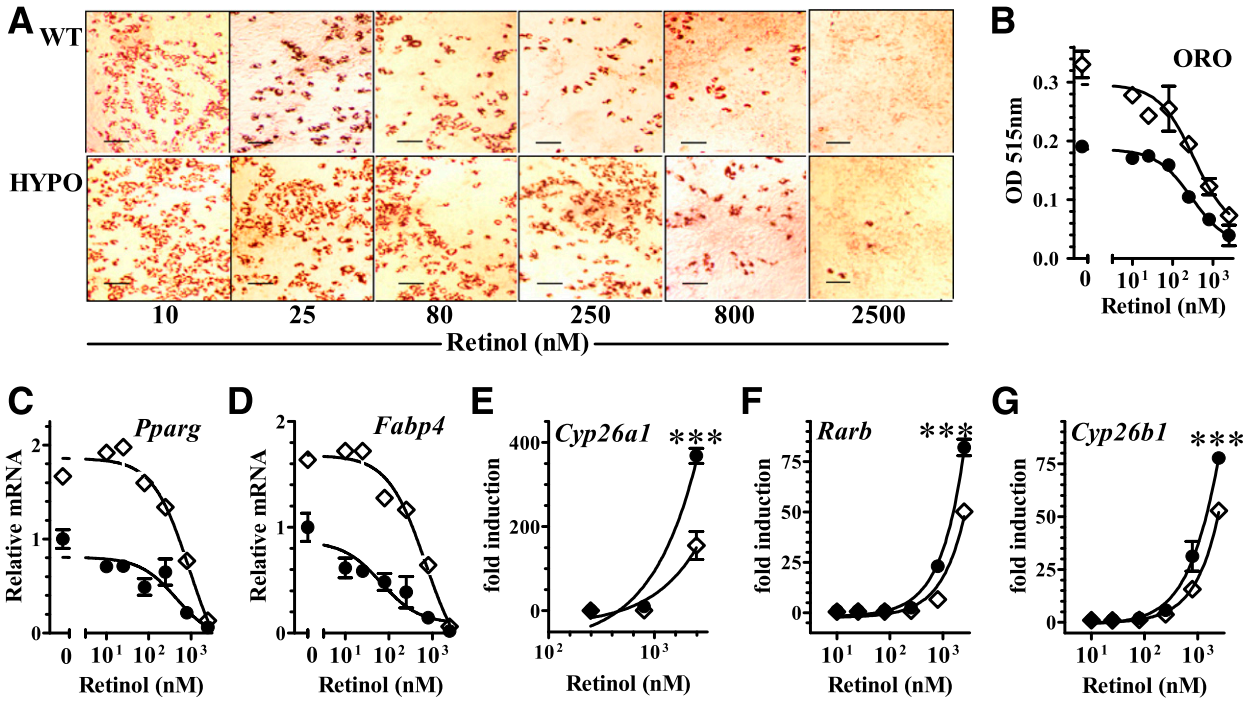


**Figure 2**—*Rdh10* HYPO MEFs are less sensitive to retinol than WT. *A*: Oil Red O (ORO) images of WT and HYPO MEFs treated with retinol every 24 h during differentiation imaged on dd7. Scale bars, 100 μm. *B–G*: Open diamonds, HYPO; filled circles, WT. *B*: Quantification of Oil Red O from *A*. MEFs from three embryos per group per dose. Two-way ANOVA, $P < 0.0001$, genotype and dose. OD, optical density. *C–G*: WT and HYPO MEFs treated with retinol as illustrated in *A* and *B*. Cells were harvested on dd7. Representative data of two experiments, each performed with duplicate cultures of MEFs from individual pups. *C* and *D*: Two-way ANOVA, $P < 0.0001$, genotype and dose. *E–G*: ***$P < 0.001$.

studied because homozygotes are not viable. Decreases in *Rdh10* mRNA in liver (52%), inguinal white adipose tissue (iWAT; 87%), and epididymal WAT (eWAT; 64%) verified knockdown (Fig. 3*A*). *Rdh10*$^{+/-}$ mice fed an LFD did not differ from WT in weight, fat body mass, or GTT (Supplementary Fig. 4). *Rdh10*$^{+/-}$ mice fed an HFD displayed substantial weight differences relative to WT (Fig. 3*B* and *C*). Males weighed >5 g more than WT littermates, whereas females weighed ~4.7 g more. Increases in body weight were caused primarily by increases in fat, with no significant differences (<1 g) in lean weight (Fig. 3*D*). No significant differences occurred in food intake between *Rdh10*$^{+/-}$ and WT (Supplementary Fig. 5). *Rdh10*$^{+/-}$ males did not differ from WT in energy expenditure or activity during light or dark cycles, normalized to lean body mass (Supplementary Fig. 6). GTT and ITT revealed glucose intolerance and insulin resistance compared with WT (Fig. 3*E* and *F*). Serum insulin increased nearly twofold in *Rdh10*$^{+/-}$ males (Fig. 3*G*). A 3.5-fold increase in serum leptin and a 40% increase in NEFA reflect increased fat mass (Fig. 3*H* and *I*). A lack of difference in GTT between WT and *Rdh10*$^{+/-}$ fed an LFD suggests that changes in glucose sensitivity were secondary to adiposity in the mice fed the HFD.

Modest decreases in atRA caused the phenotype (Fig. 3*J*). Tissue atRA concentrations decreased by 25% or less: liver 23 and 20% for males and females, respectively; epididymal/parametrial WAT 20 and 25%; and femoral WAT 15 and 15%. Tissue atRA was normalized to tissue weight; normalizing to protein had a tissue-specific effect because of changes in total protein as well as fat mass (Supplementary Fig. 7).

### Fat Pad Abnormalities

eWAT, iWAT, and perirenal WAT were enlarged in *Rdh10*$^{+/-}$ males fed an HFD (Fig. 4*A*). eWAT of *Rdh10*$^{+/}$ males have a 73% decrease in *Adipoq*, an indicator of function, but increased expression of the hypoxia-induced gene *Hif1a* and the fibrosis indicator *Col6a1*, a target of *Hif1a*. *Pparg* was reduced 50%, a decrease that reflects an increase in Hif1a (Fig. 4*B*) (27). The inflammatory indicators *Saa3* and *Tnfa* increased two- to threefold. *Rdh10*$^{+/-}$ mice had larger adipocytes in eWAT and iWAT (Fig. 4*C*, *D*, and *F*), reflected in the average adipocyte sizes (Fig. 4*E* and *G*). Histologically, *Rdh10*$^{+/-}$ males also had increased inflammation (Fig. 4*H*) and fibrosis (Fig. 4*I*). These results suggest that adipose expansion exceeds angiogenesis, which induces hypoxia, inflammation, oxidative stress, and fibrosis (28). Fibrosis from persistent inflammation damages adipocytes, which increases NEFA release, resulting in nonadipose tissues accumulating TAG. The inflammation and fibrosis of adipose, with the increase in serum NEFA (Fig. 3*I*), would contribute to liver steatosis.

### Males Fed an HFD Develop Liver Steatosis

Histological analysis showed that 14 of 19 (~74%) *Rdh10*$^{+/-}$ males fed an HFD had increased fat accumulation in liver, relative to 7 of 18 (39%) WT, without enhancement of the inflammation marker F4/80 (Fig. 5*A*). Females fed the HFD

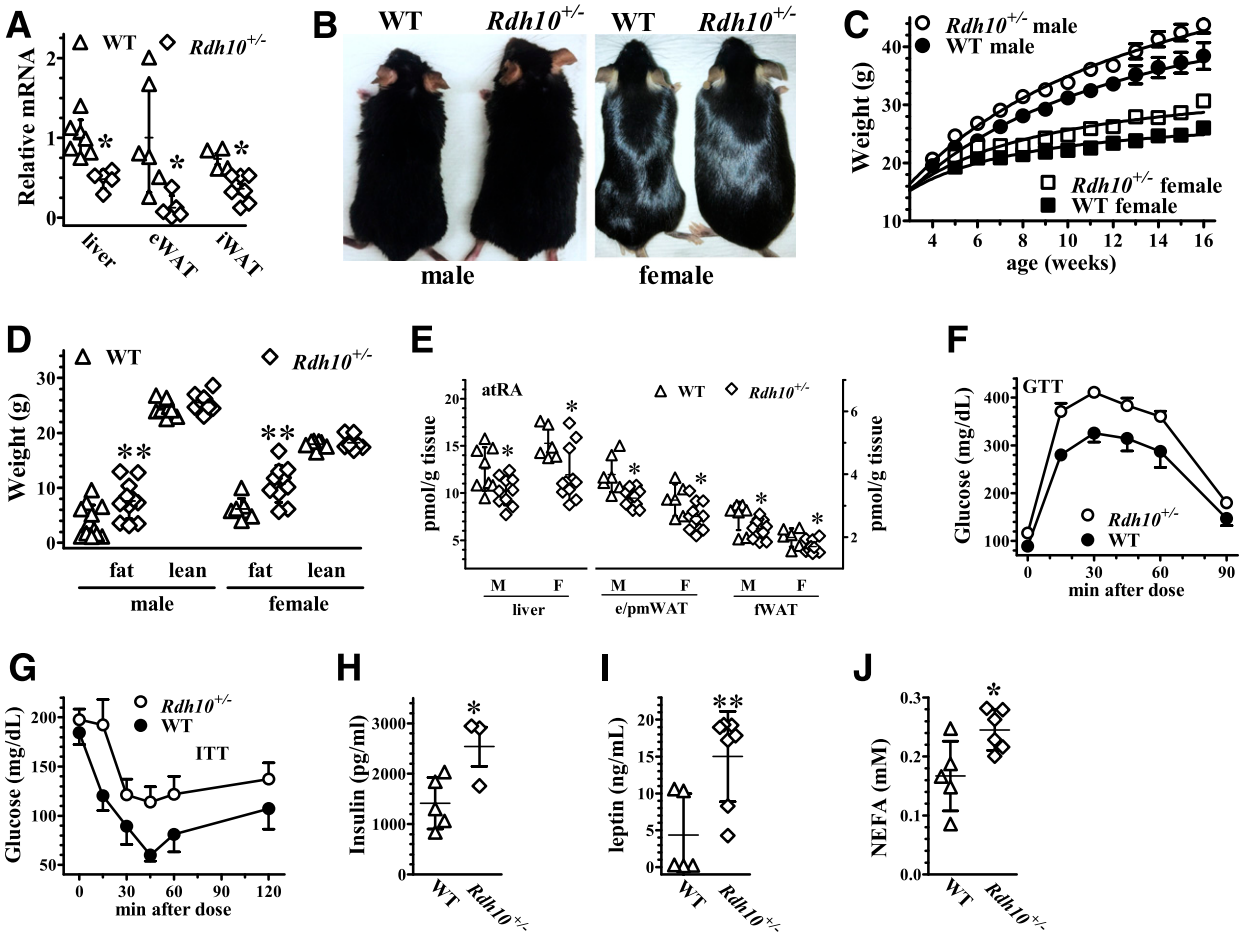


**Figure 3**—*A*: *Rdh10* mRNA decreases in tissues of male *Rdh10*$^{+/-}$ mice: $n$ = 4–7 each per genotype. *$P < 0.03$. *B*: Representative images of WT and *Rdh10*$^{+/-}$ mice. *C*: Body weights. Males: $n$ = 12–33 WT; $n$ = 11–30 *Rdh10*$^{+/-}$. Females: $n$ = 11 WT; $n$ = 10 *Rdh10*$^{+/-}$. Two-way-ANOVA, $P <$ 0.0001, males and females, genotype and age. *D*: Body compositions by Echo MRI. Males: $n$ = 11 WT; $n$ = 12 *Rdh10*$^{+/-}$. Females: $n$ = 7 WT; $n$ = 10 *Rdh10*$^{+/-}$. **$P < 0.009$. *E*: atRA tissue concentrations: 7–11 mice per group. *$P < 0.04$. Liver, left $y$-axis; WAT, right $y$-axis. e/pmWAT, epididymal/parametrial WAT; fWAT, femoral WAT. *F*: GTT: $n$ = 5 WT; 7 *Rdh10*$^{+/-}$. Representative data from three experiments. Significant difference for genotype by two-way ANOVA, $P < 0.0001$. *G*: ITT: $n$ = 6 WT; 10 *Rdh10*$^{+/-}$. Representative data from three experiments. Significant difference for genotype by two-way-ANOVA, $P = 0.0004$. *H*: Serum insulin; $n$ = 3–5 mice per group. *$P < 0.04$. *I*: Serum leptin; $n$ = 5–7 mice per group. **$P < 0.01$. *J*: Serum NEFAs; $n$ = 5–7 mice per group. *$P = 0.05$.

showed a much more modest reaction (Fig. 5*B*). *Rdh10*$^{+/-}$ males fed the HFD had a greater than twofold increase (5.2 mg) in liver TAG compared with WT (Fig. 5*C*). Three of the *Rdh10*$^{+/-}$ males reacted more intensely than the others. Excluding these three from the analysis still showed a significant difference from WT, with a 44% increase in TAG ($P < 0.02$). In contrast, livers of female *Rdh10*$^{+/-}$ fed an HFD showed no significant difference in TAG content from WT (Fig. 5*D*). *Rdh10*$^{+/-}$ male livers were larger than WT (Fig. 5*E*), weighing ~20% more (0.2 g) (Fig. 5*E* and *G*). *Rdh10*$^{+/-}$ female liver weights did not differ from WT ($P >$ 0.1) (Fig. 5*F*). Decreases in gene expression occurred in *Acadm* (52% decrease), which encodes the medium-chain acyl-CoA dehydrogenase; *Ppara* (32% decrease), which stimulates β-oxidation; and *Saa1* (63% decrease), which designates acute inflammation (Fig. 5*H*). Serum β-hydroxybutyrate in fasted males and females did not differ with genotype (Supplementary Fig. 8).

### Increased Adipocyte Formation in Female Femur Marrow

We examined femur bone marrow, because marrow stem cells serve as progenitors to adipocytes. *Rdh10*$^{+/-}$ males fed an HFD had a slight increase in adipocytes near the growth plate, which was not statistically significant (Fig. 6*A* and *B*), and showed no significant differences in genes typically expressed in adipocytes (Fig. 6*C*). Females fed an HFD had a threefold increase in adipocytes clustered near the growth plate (Fig. 6*D* and *E*) and enhanced expression of *Fabp4* (>50%), *Pparg* (~100%), *Fabp5* (100%), and *AdipoQ* (>80%) (Fig. 6*G*). Females fed an LFD also had threefold increased adipocytes in femur marrow (Fig. 6*H* and *I*). Increased expression of *AdipoQ* did not increase circulating adiponectin (Supplementary Fig. 9). Femur lengths of males did not differ with genotype, but femurs from the *Rdh10*$^{+/-}$ females fed an HFD were ~8.5% longer than WT (Fig. 6*J*).

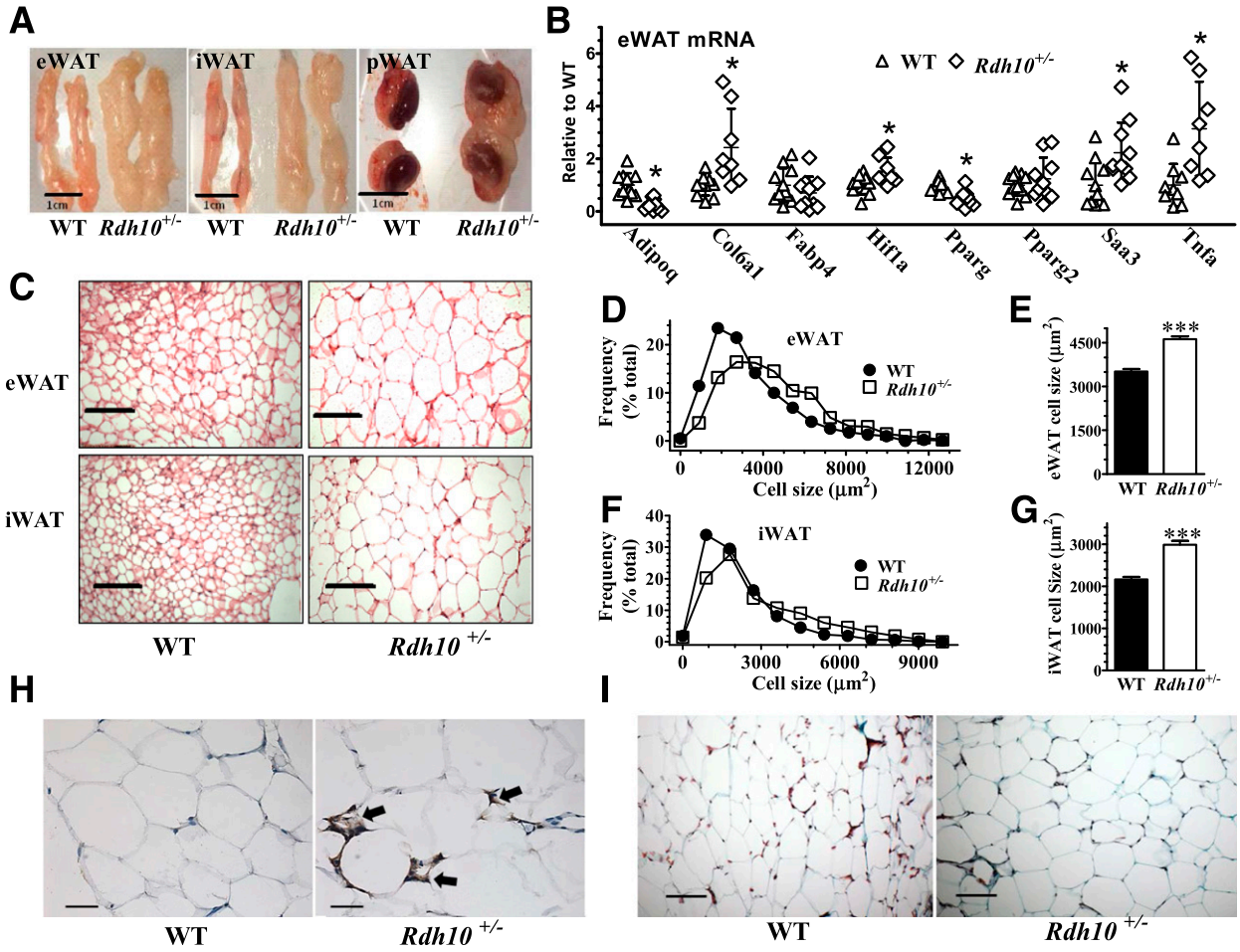


**Figure 4**—Increased fat pads and adipocyte sizes and gene expression changes in *Rdh10*$^{+/-}$ mice. *A*: Representative images of WAT depots. p, perirenal. *B*: Indicators of adipocyte differentiation (*Pparg* and *Fabp4*), adipocyte function (*Adipoq* and *Hif1a*), inflammation (*Saa3* and *Tnfa*), and fibrosis (*Co16a1*) ($n$ = 8–11 mice). *$P < 0.02$. *C*: Representative images of WAT (H-E staining). WT, $n$ = 13; *Rdh10*$^{+/-}$, $n$ = 11. Scale bars, 200 μm. *D*: Cell size distribution of eWAT. *E*: Average cell size of eWAT. ***$P < 0.001$. *F*: Cell size distribution of iWAT. *G*: Average cell size of iWAT. ***$P < 0.001$. *H*: Representative images of F4/80 stain for macrophages in eWAT; $n$ = 5–6 mice. Scale bars, 50 μm. Arrows denote macrophages. *I*: Representative images of trichrome stain for fibrosis in eWAT; $n$ = 5–6 mice. Scale bars, 50 μm.

### atRA Rescues the Phenotype

atRA caused a greater than fivefold decrease in the number of Oil Red O–positive cells in HYPO MEFs and a greater than threefold decrease in WT, and suppressed differentiation to a similar base value in both (Fig. 7*A* and *B*). *Pparg* and *Fabp4* expression was 4- and 14-fold higher in HYPO MEFs than WT, which was reduced by atRA to 4- and 12-fold less than vehicle-treated HYPO MEFs (Fig. 7*C* and *D*). Because atRA activates both RAR and PPARδ, we tested receptor-specific ligands in CKO MEFs, which differentiated to a much greater extent than WT (Fig. 7*E* and *F*). The RAR pan-agonist TTNPB reduced differentiation by fivefold, whereas the PPARδ agonist was ineffective. TTNPB also reduced *Pparg* and *Fabp4* expression by 5- and 40-fold, respectively (Fig. 7*G* and *H*). Thus, HYPO and CKO MEFs respond robustly to atRA with robust decreases in adipogenesis.

We next determined the impact of atRA on *Rdh10*$^{+/-}$ mice fed an HFD. Six-week-old mice were implanted with atRA timed-release capsules. By the end of week 9, *Rdh10*$^{+/-}$ mice treated with low-dose atRA weighed 9 g less than placebo-treated mice and had body weights equivalent to mice fed an LFD (Fig. 7*I*). atRA dosing also improved glucose tolerance and insulin sensitivity (Fig. 7*J* and *K*). A 50% decrease in fat relative to vehicle-treated mice reflected the major weight difference, with no significant change in lean mass (Fig. 7*L*). atRA rescued the liver steatosis phenotype and reduced the sizes of white adipocytes in eWAT (Fig. 7*M*). These data suggest the potential of chronic low-dose atRA treatment for metabolic disorders.

## DISCUSSION

We undertook this research to reveal postnatal Rdh10 contributions to atRA function and to assess endogenous atRA actions. Previous studies focusing on specific organs or using vitamin A deficiency models revealed that atRA has widespread impact on metabolism, consistent with organ

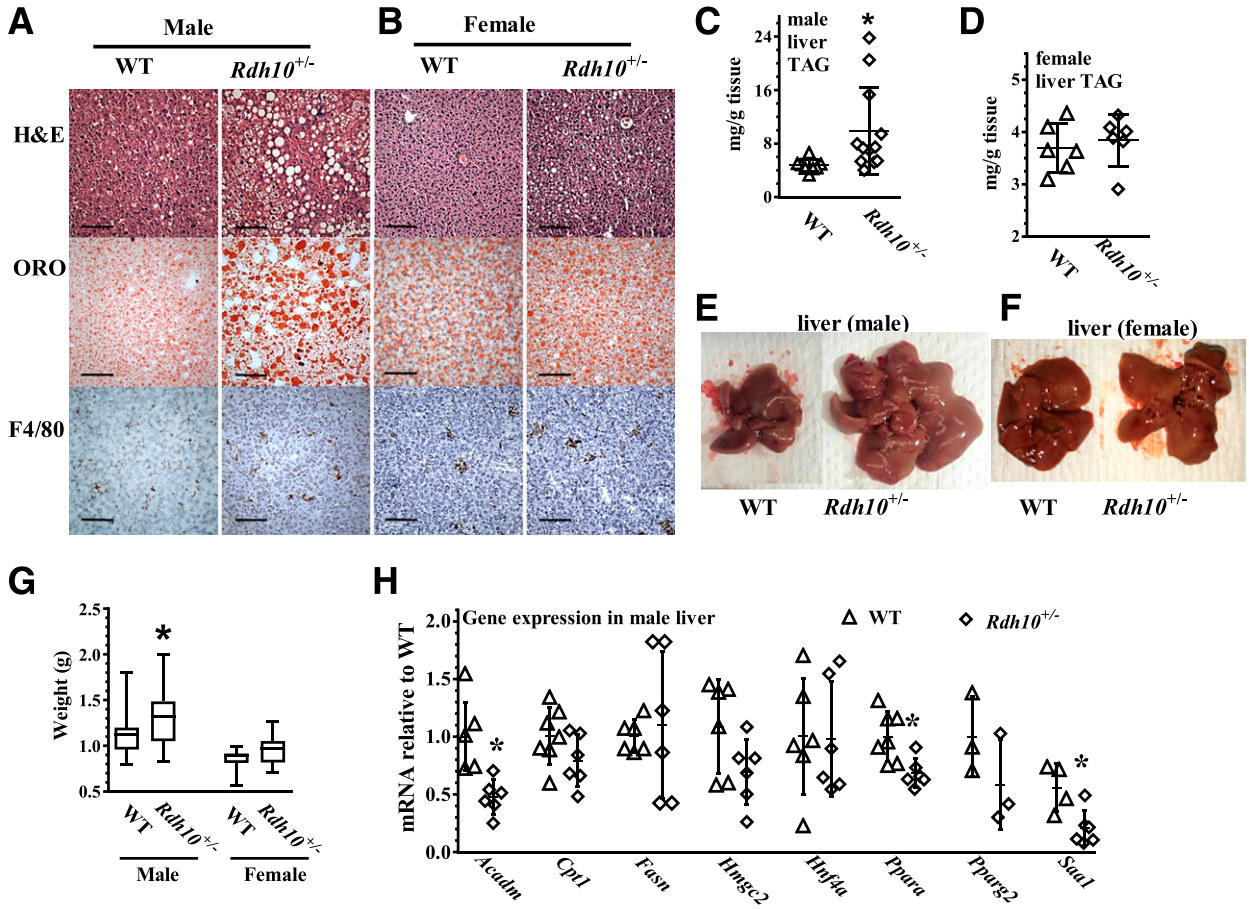


**Figure 5**—*Rdh10*$^{+/-}$ mice develop fatty livers. *A* and *B*: H-E, Oil Red O (ORO), and F4/80 immunohistochemistry. Representative images of three groups; $n$ = 4–6 mice per group per genotype. *A*: Males. *B*: Females. Scale bars, 130 μm. *C* and *D*: Liver TAG quantification. *C*: Males, $n$ = 8–12 per genotype. *$P < 0.04$. *D*: Females, $n$ = 6 per genotype. *E* and *F*: Representative liver images. *E*: Males. *F*: Females. *G*: Liver weights. Males, $n$ = 32–39 per genotype; females, $n$ = 8–10 per genotype. *$P < 0.05$. *H*: Expression of liver genes in males; $n$ = 6–7 per genotype. Representative result of two groups. *$P < 0.02$.

autonomous effects (15–17,20,29–32). Total *Rdh10* ablation impairs the biogenesis of multiple organs, including the pancreas, and causes embryonic lethality between E10.5 and E13, but *Rdh10*$^{+/-}$ mice reportedly were "indistinguishable" from WT (33). This conclusion, referring to the appearance of mice fed a chow diet, coincides with our observations of the appearance of *Rdh10*$^{+/-}$ mice fed an LFD.

Despite evaluating heterozygotes, the metabolic phenotype reported here involved multiple tissues and was surprisingly severe. More surprising were the modest decreases in tissue atRA that led to the metabolic defects. This reveals that minor decreases in tissue atRA have a major impact on metabolic health and can predispose to obesity, glucose intolerance, insulin resistance, and ectopic adipose formation and fat deposition. This finding, as well as rescue with low-dose atRA, indicates the importance of establishing the connection between retinol activation and atRA concentrations and metabolic diseases, and suggests the potential of low-dose atRA for metabolic disease therapy.

Our observations support the proposed functions of atRA in arresting adipogenesis and regulating lipid metabolism (19,21). Previous studies to define atRA function in energy homeostasis, however, were performed either with established cell lines, which may not faithfully model their origins, or through dosing pharmacological and/or toxic amounts of atRA to animals fed a diet copious in vitamin A (lab chow). Diets with copious vitamin A obscure knockout effects and could contribute to vitamin A toxicity when dosing pharmacological atRA (19,34). Vitamin A and atRA represent prototypical examples of hormesis, an inverted U-shaped dose-response curve in which increasing concentrations increase beneficial effects to a point, but beneficial effects ultimately subside with high concentrations and toxicity ensues. Thus, dosing high amounts of atRA confounds toxicology with physiology, especially in animals fed chow diets, which contain at least fourfold more vitamin A than used here, which we based on recommendations by the National Research Council.

The dimorphic impact of atRA exposed another unanticipated result. Distinctions between males and females

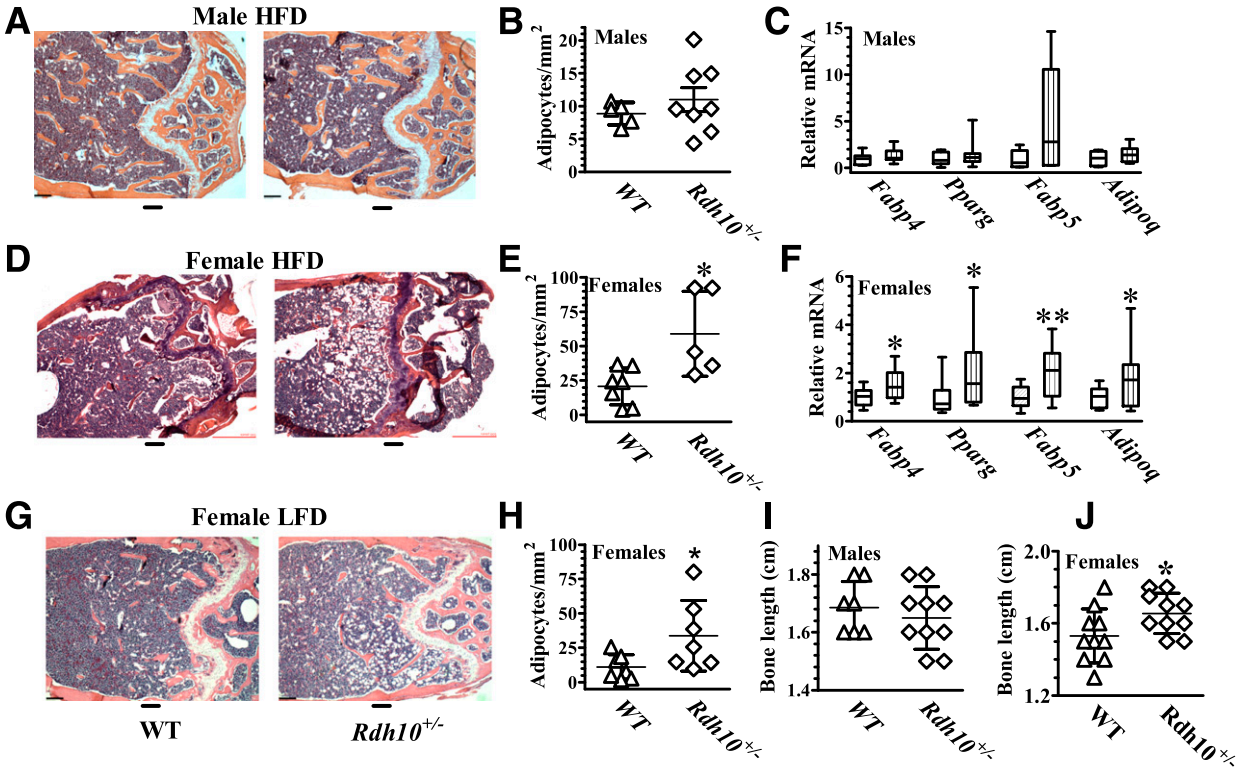


**Figure 6**—Loss of Rdh10 in bone marrow increases bone marrow adipocyte formation. *A*, *D*, and *G*: H-E imaging of femurs. *A*: Males, HFD. *D*: Females, HFD. *G*: Females, LFD. Scale bars, 500 μm. *B*, *E*, and *H*: Adipocyte numbers in *A*, *D*, and *G*. *B*: Males, $n$ = 5–8 per genotype. *E*: Females, $n$ = 5–7 per genotype. *$P < 0.02$. *H*: Females, $n$ = 7 per genotype. *$P < 0.05$. *C*: Expression of adipocyte markers in bone marrow. Males, HFD. $n$ = 7 WT, open boxes; $n$ = 11 *Rdh10*$^{+/-}$, striped boxes. *F*: Expression of adipocyte markers in bone marrow, females, HFD. $n$ = 11–13 per genotype. *$P < 0.04$; **$P < 0.01$. *I* and *J*: Femur lengths. Males: $n$ = 7 WT; $n$ = 10 *Rdh10*$^{+/-}$. Females (HFD): $n$ = 10 per genotype. *$P <$ 0.05.

in diet-dependent liver steatosis and bone marrow adipocyte formation provide new insight into interaction(s) between retinoids and steroid sex hormones. Complex interactions between the two estrogen receptors ERα and ERβ and the atRA receptors RARα and RARβ occur in breast cancer cell lines (35,36). Moreover, estrogen induces atRA biosynthesis in primary human endometrial cells (37), whereas atRA induces estrogen biosynthesis in placental cells (38). Little is known about these interactions in adipose. atRA plus estrogen, however, additively induce *Rarg*, estrogen receptor β (*Esr2*), and aromatase (*Cyp19a1*) in NIH3T3-L1 cells (39). It is reasonable to propose that atRA impairs estrogen function in female bone marrow, in addition to having direct effects. Interactions between androgens and atRA also occur. atRA downregulates androgen receptor mRNA in breast cancer cell lines. Vitamin A restriction increases androgen receptor expression in rat testis (40). Castration increases *Rara* and *Rarg* mRNAs in rat prostate, which testosterone dosing represses (41). Testosterone reduces loss of bone density in mice dosed chronically with pharmacological atRA (10 mg/kg/day) (42). These interactions might contribute to differences in the bone phenotype between male and female *Rdh10*$^{+/-}$ mice.

Meta-analysis of epidemiological studies indicate a U-shaped relationship between serum retinol and hip fracture risk (hormesis), i.e., either high or low serum retinol increases osteoporosis risk (43). Skeletal growth relies on RAR. Excess atRA accelerates bone maturation and decreases bone density, especially in orchiectomized rodents (29,42). The mechanism seems related to atRA effects on multipotent stem cells in bone marrow differentiating into osteoblasts or adipocytes. Increased marrow adiposity associates with adverse effects on skeletal function (44); atRA may provide a link in this connection. Multiple studies with cell lines demonstrate that atRA inhibits mesenchymal cell differentiation into adipocytes and promotes differentiation into osteoblasts, and indicate that adipocyte formation impairs osteoblast production (30,45). Increased adipocyte differentiation during osteoporosis may contribute to bone deterioration by occupying the marrow niche and by reducing osteoblastogenesis. A recent study, using primary bone marrow stem cells, extended the observation that atRA inhibits adipocyte differentiation but concluded that atRA inhibits osteoblast differentiation (46). Our study did not address adipogenesis versus osteoblastogenesis but showed that a decrease in endogenous atRA stimulates adipocyte formation in bone marrow independently of dietary fat that affects females. Thus, the *Rdh10*$^{+/-}$ mouse introduces a model for studying adipocyte formation in bone marrow and atRA effects on osteoblastogenesis and osteoporosis.

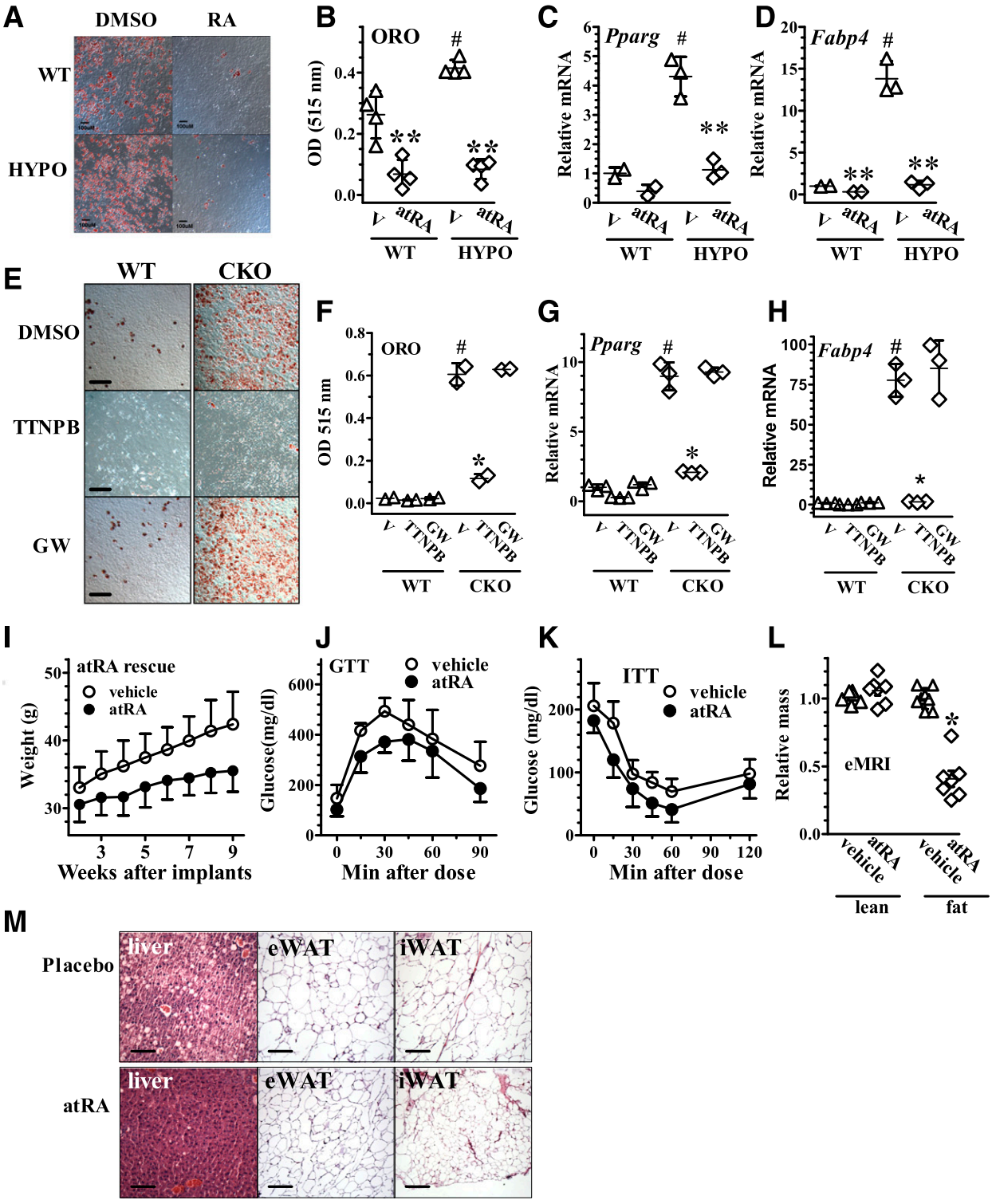


**Figure 7**—atRA through RAR ameliorates excess adipogenesis. *A*: Oil Red O imaging of MEFs differentiated in the presence of vehicle or atRA. MEFs from four embryos per genotype. Representative result of two experiments. Scale bars, 100 μm. *B*: Quantification of Oil Red O (ORO) in *A*. $^{**}P < 0.006$ from vehicle (V); #$P < 0.01$, WT vs. HYPO. *C* and *D*: Expression of adipogenic genes (*Pparg* and *Fabp4*) in MEFs differentiated in the presence of vehicle or atRA; $n = 2$–3 embryos per group. Representative result of two experiments. $^{**}P < 0.006$ from vehicle; #$P < 0.008$, WT vs. HYPO. *E*: Oil Red O images of differentiated CKO on dd7 treated with vehicle, TTNPB, or GW0742 throughout differentiation. Representative result of two experiments with duplicates for each. Scale bars, 200 μm. *F*: Quantification of images in *E*. #,$^{*}P < 0.007$ from WT and vehicle-treated CKO, respectively. *G* and *H*: Expression of *Pparg* and *Fabp4* in cells in *E*. Representative result of two experiments. $n = 3$ per group per experiment. #,$^{*}P < 0.007$ from WT and vehicle-treated CKO, respectively. *I* and *J*: *Rdh10*$^{+/-}$ mice fed an HFD and treated with time-released placebo or atRA. $n = 6$–7 mice per genotype. *I*: Body weights. Two-way ANOVA, dose and time, $P < 0.0001$. *J*: GTT, two-way ANOVA, dose and time, $P < 0.0001$. *K*: ITT, two-way ANOVA, dose and time, $P < 0.0001$. *L*: EchoMRI (eMRI). Fat: $^{*}P < 0.0001$, placebo vs. atRA. *M*: Representative H-E images of tissues. Scale bars, 130 μm. OD, optical density.

The relationship of retinol and atRA with liver steatosis has been unclear. Some reports concluded that RAR induces liver steatosis, whereas others reported beneficial actions; this may reflect retinoid hormesis causing dose-dependent outcomes (47). The intervention of specific atRA receptors offers some clarity. Transgenic male mice that express a dominant-negative RARα develop liver steatosis by 4 months old without obesity and develop hepatocarcinoma by 12 months (48). The former was associated with decreased fatty acid oxidation. Overexpression of the atRA-inducible RARβ in mouse liver enhances fatty acid oxidation and energy expenditure (31), whereas the RARβ2-specific agonist AC261066 reduces liver steatosis in HFD-fed mice (49). Increasing endogenous atRA concentrations by inhibiting the atRA-catabolic *Cyp26* isozymes enhances expression of mitochondrial biogenesis markers *Nrf1* and *Pgc1β* 5- to 10-fold (32). These data are consistent with atRA enhancing fatty acid oxidation and mitochondrial biogenesis in vivo and suggest processes contributing to the liver steatosis phenotype.

In contrast to increased adiposity of *Rdh1* and *Rdh10* knockouts, *Raldh1*-knockout mice resist adiposity. *Raldh1* ablation decreases atRA in liver and in some female fat pads of 6- to 7-week-old mice fed an HFD, which should enhance adiposity but does not affect retinal in these mice. These and other data indicate that the multifunctional Raldh1, which also has a diverse array of substrates, acts independently of retinal and RA in adipose to permit adiposity (50).

These studies provide the first insight into the physiological effects of endogenous atRA in energy balance and the function of Rdh10 in postnatal intermediary metabolism. The data reveal that Rdh10 contributes to normal glucose and insulin sensitivity, control of adiposity and adipogenesis, and preservation of bone health. The surprisingly modest decrease in atRA that caused these effects suggests that low-dose atRA therapy may help ameliorate adiposity and its sequelae of glucose intolerance and insulin resistance.

**Acknowledgments.** The authors thank Steven Ruzin and Denise Schichness (Biological Imaging Facility, UC Berkeley) for exceptional support of this project, Charles Krois for insightful discussions, James Olzmann and Truc Nguyen for generating immortalized MEF cells, and Anh Hoang Nguyen and Yanxin Wu Madrid (all UC Berkeley) for technical support.

**Funding.** This research was supported by grants from the National Institutes of Health (DK102014 and DK090522), the UC Berkeley College of Natural Resources Sponsored Projects for Undergraduate Research (C.P.S., M.K., C.P.-S.L., E.D., and M.T.), the UC Berkeley Rose Hills Foundation (M.T.), and the National Natural Science Foundation of China (grant 21405036 to Y.D.).

**Duality of Interest.** No potential conflicts of interest relevant to this article were reported.

**Author Contributions.** D.Y. contributed to experimental design, performed experiments, analyzed and interpreted data, and contributed to writing and editing the manuscript. M.G.V. contributed to experimental design, analyzed and interpreted data, and contributed to editing the manuscript. C.P.S., M.K., C.P.-S.L., E.D., H.S.Y., M.T., and Y.D. performed experiments and analyzed and interpreted data. J.L.N. contributed to experimental design, analyzed and interpreted data, and contributed to writing and editing the manuscript. D.Y. and J.L.N. are the guarantors of this work and, as such, had full access to all the data in the study and take responsibility for the integrity of the data and the accuracy of the data analysis.

## References

1. Iskakova M, Karbyshev M, Piskunov A, Rochette-Egly C. Nuclear and extra-nuclear effects of vitamin A. Can J Physiol Pharmacol 2015;93:1065–1075
2. Napoli JL. Physiological insights into all-trans-retinoic acid biosynthesis. Biochim Biophys Acta 2012;1821:152–167
3. Kedishvili NY. Retinoic acid synthesis and degradation. Subcell Biochem 2016;81:127–161
4. Harrison EH. Mechanisms involved in the intestinal absorption of dietary vitamin A and provitamin A carotenoids. Biochim Biophys Acta 2012;1821:70–77
5. Ross AC, Zolfaghari R. Cytochrome P450s in the regulation of cellular retinoic acid metabolism. Annu Rev Nutr 2011;31:65–87
6. Nelson CH, Buttrick BR, Isoherranen N. Therapeutic potential of the inhibition of the retinoic acid hydroxylases CYP26A1 and CYP26B1 by xenobiotics. Curr Top Med Chem 2013;13:1402–1428
7. Zhai Y, Higgins D, Napoli JL. Coexpression of the mRNAs encoding retinol dehydrogenase isozymes and cellular retinol-binding protein. J Cell Physiol 1997; 173:36–43
8. Niederreither K, Vermot J, Fraulob V, Chambon P, Dolle P. Retinaldehyde dehydrogenase 2 (RALDH2)–independent patterns of retinoic acid synthesis in the mouse embryo. Proc Natl Acad Sci U S A 2002;99:16111–16116
9. Dupé V, Matt N, Garnier JM, Chambon P, Mark M, Ghyselinck NB. A newborn lethal defect due to inactivation of retinaldehyde dehydrogenase type 3 is prevented by maternal retinoic acid treatment. Proc Natl Acad Sci U S A 2003;100:14036–14041
10. Wu BX, Chen Y, Chen Y, et al. Cloning and characterization of a novel all-trans retinol short-chain dehydrogenase/reductase from the RPE. Invest Ophthalmol Vis Sci 2002;43:3365–3372
11. Wu BX, Moiseyev G, Chen Y, Rohrer B, Crouch RK, Ma JX. Identification of RDH10, an all-trans retinol dehydrogenase, in retinal Muller cells. Invest Ophthalmol Vis Sci 2004;45:3857–3862
12. Romand R, Kondo T, Cammas L, Hashino E, Dollé P. Dynamic expression of the retinoic acid-synthesizing enzyme retinol dehydrogenase 10 (rdh10) in the developing mouse brain and sensory organs. J Comp Neurol 2008;508: 879–892
13. Rhinn M, Schuhbaur B, Niederreither K, Dollé P. Involvement of retinol dehydrogenase 10 in embryonic patterning and rescue of its loss of function by maternal retinaldehyde treatment. Proc Natl Acad Sci U S A 2011;108:16687–16692
14. Ashique AM, May SR, Kane MA, et al. Morphological defects in a novel Rdh10 mutant that has reduced retinoic acid biosynthesis and signaling. Genesis 2012;50: 415–423
15. Bonney S, Harrison-Uy S, Mishra S, et al. Diverse functions of retinoic acid in brain vascular development. J Neurosci 2016;36:7786–7801
16. Tong MH, Yang QE, Davis JC, Griswold MD. Retinol dehydrogenase 10 is indispensible for spermatogenesis in juvenile males. Proc Natl Acad Sci U S A 2013; 110:543–548
17. Lee SA, Belyaeva OV, Wu L, Kedishvili NY. Retinol dehydrogenase 10 but not retinol/sterol dehydrogenase(s) regulates the expression of retinoic acid-responsive genes in human transgenic skin raft culture. J Biol Chem 2011;286:13550–13560
18. Wang C, Kane MA, Napoli JL. Multiple retinol and retinal dehydrogenases catalyze all-trans-retinoic acid biosynthesis in astrocytes. J Biol Chem 2011;286: 6542–6553
19. Zhang M, Hu P, Krois CR, Kane MA, Napoli JL. Altered vitamin A homeostasis and increased size and adiposity in the rdh1-null mouse. FASEB J 2007;21:2886–2896
20. Amengual J, Ribot J, Bonet ML, Palou A. Retinoic acid treatment enhances lipid oxidation and inhibits lipid biosynthesis capacities in the liver of mice. Cell Physiol Biochem 2010;25:657–666

21. Berry DC, DeSantis D, Soltanian H, Croniger CM, Noy N. Retinoic acid upregulates preadipocyte genes to block adipogenesis and suppress diet-induced obesity. Diabetes 2012;61:1112–1121
22. Kelly NH, Schimenti JC, Patrick Ross F, van der Meulen MC. A method for isolating high quality RNA from mouse cortical and cancellous bone. Bone 2014;68:1–5
23. Xu J. Preparation, culture, and immortalization of mouse embryonic fibroblasts. Curr Protoc Mol Biol 2005;Chapter 28:Unit 28.1
24. Kane MA, Folias AE, Napoli JL. HPLC/UV quantitation of retinal, retinol, and retinyl esters in serum and tissues. Anal Biochem 2008;378:71–79
25. Kane MA, Folias AE, Wang C, Napoli JL. Quantitative profiling of endogenous retinoic acid in vivo and in vitro by tandem mass spectrometry. Anal Chem 2008;80:1702–1708
26. Ran FA, Hsu PD, Wright J, Agarwala V, Scott DA, Zhang F. Genome engineering using the CRISPR-Cas9 system. Nat Protoc 2013;8:2281–2308
27. Halberg N, Khan T, Trujillo ME, et al. Hypoxia-inducible factor 1alpha induces fibrosis and insulin resistance in white adipose tissue. Mol Cell Biol 2009;29:4467–4483
28. Kusminski CM, Bickel PE, Scherer PE. Targeting adipose tissue in the treatment of obesity-associated diabetes. Nat Rev Drug Discov 2016;15:639–660
29. Nilsson O, Isoherranen N, Guo MH, et al. Accelerated skeletal maturation in disorders of retinoic acid metabolism: a case report and focused review of the literature. Horm Metab Res 2016;48:737–744
30. Skillington J, Choy L, Derynck R. Bone morphogenetic protein and retinoic acid signaling cooperate to induce osteoblast differentiation of preadipocytes. J Cell Biol 2002;159:135–146
31. Li Y, Wong K, Walsh K, Gao B, Zang M. Retinoic acid receptor β stimulates hepatic induction of fibroblast growth factor 21 to promote fatty acid oxidation and control whole-body energy homeostasis in mice. J Biol Chem 2013;288:10490–10504
32. Tripathy S, Chapman JD, Han CY, et al. All-trans-retinoic acid enhances mitochondrial function in models of human liver. Mol Pharmacol 2016;89:560–574
33. Arregi I, Climent M, Iliev D, et al. Retinol dehydrogenase-10 regulates pancreas organogenesis and endocrine cell differentiation via paracrine retinoic acid signaling. Endocrinology 2016;157:4615–4631
34. E X, Zhang L, Lu J, et al. Increased neonatal mortality in mice lacking cellular retinol-binding protein II. J Biol Chem 2002;277:36617–36623
35. Rousseau C, Nichol JN, Pettersson F, Couture MC, Miller WH Jr. ERbeta sensitizes breast cancer cells to retinoic acid: evidence of transcriptional crosstalk. Mol Cancer Res 2004;2:523–531
36. White KA, Yore MM, Deng D, Spinella MJ. Limiting effects of RIP140 in estrogen signaling: potential mediation of anti-estrogenic effects of retinoic acid. J Biol Chem 2005;280:7829–7835
37. Deng L, Shipley GL, Loose-Mitchell DS, et al. Coordinate regulation of the production and signaling of retinoic acid by estrogen in the human endometrium. J Clin Endocrinol Metab 2003;88:2157–2163
38. Zhu SJ, Li Y, Li H, et al. Retinoic acids promote the action of aromatase and 17beta-hydroxysteroid dehydrogenase type 1 on the biosynthesis of 17beta-estradiol in placental cells. J Endocrinol 2002;172:31–43
39. Shearer KD, Morrice N, Henderson C, et al. Fenretinide prevents obesity in aged female mice in association with increased retinoid and estrogen signaling. Obesity (Silver Spring) 2015;23:1655–1662
40. Zhuang YH, Bläuer M, Ylikomi T, Tuohimaa P. Spermatogenesis in the vitamin A-deficient rat: possible interplay between retinoic acid receptors, androgen receptor and inhibin alpha-subunit. J Steroid Biochem Mol Biol 1997;60:67–76
41. Huang HF, Li MT, Von Hagen S, Zhang YF, Irwin RJ. Androgen modulation of the messenger ribonucleic acid of retinoic acid receptors in the prostate, seminal vesicles, and kidney in the rat. Endocrinology 1997;138:553–559
42. Broulík PD, Raška I, Brouliková K. Prolonged overdose of all-trans retinoic acid enhances bone sensitivity in castrated mice. Nutrition 2013;29:1166–1169
43. Wu AM, Huang CQ, Lin ZK, et al. The relationship between vitamin A and risk of fracture: meta-analysis of prospective studies. J Bone Miner Res 2014;29:2032–2039
44. Veldhuis-Vlug AG, Rosen CJ. Mechanisms of marrow adiposity and its implications for skeletal health. Metabolism 2017;67:106–114
45. Zhang W, Deng ZL, Chen L, et al. Retinoic acids potentiate BMP9-induced osteogenic differentiation of mesenchymal progenitor cells. PLoS One 2010;5:e11917
46. Green AC, Kocovski P, Jovic T, et al. Retinoic acid receptor signalling directly regulates osteoblast and adipocyte differentiation from mesenchymal progenitor cells. Exp Cell Res 2017;350:284–297
47. Mellor CL, Steinmetz FP, Cronin MT. The identification of nuclear receptors associated with hepatic steatosis to develop and extend adverse outcome pathways. Crit Rev Toxicol 2016;46:138–152
48. Yanagitani A, Yamada S, Yasui S, et al. Retinoic acid receptor alpha dominant negative form causes steatohepatitis and liver tumors in transgenic mice. Hepatology 2004;40:366–375
49. Trasino SE, Tang XH, Jessurun J, Gudas LJ. Retinoic acid receptor β2 agonists restore glycaemic control in diabetes and reduce steatosis. Diabetes Obes Metab 2016;18:142–151
50. Yang D, Krois CR, Huang P, et al. Raldh1 promotes adiposity during adolescence independently of retinal signaling. PLoS One 2017;12:e0187669